FIRST DIRECT COMPARISONS OF A COTRI ANALYTICAL MODEL TO DATA FROM A SASE FEL AT 540, 265, AND 157 nm*

A.H. Lumpkin#, R.J. Dejus, and D.W. Rule†
Advanced Photon Source, Argonne, Illinois 60439 U.S.A.
†NSWC Carderock Division, West Bethesda, Maryland 20817 U.S.A.

Abstract

We have been addressing fundamental aspects of the microbunching of electron beams that are induced by the self-amplified spontaneous emission (SASE) free-electron laser (FEL) process using coherent optical transition radiation interferometry (COTRI) techniques. Over the last several years we have extended operations from the visible to the VUV regime at the Advanced Photon Source (APS) low-energy undulator test line (LEUTL) project. We have now performed our first direct comparison of the results of an analytical model to COTRI experimental data at 540, 265, and 157 nm.

INTRODUCTION

The interest in using coherent optical transition radiation interferometry (COTRI) patterns to elucidate self-amplified spontaneous emission (SASE) free-electron laser (FEL) experiments has increased as we have explored the technique's sensitivities. In the past we had only reported qualitative agreement on reproducing the main features of the far-field interferometric images [1-3]. As an exercise to develop our understanding and to test our COTRI analytical model [4], test cases from the APS SASE FEL data at wavelengths of 540, 265, and 157 nm were evaluated. Although the beam energy is the main parameter change, the relative angular pattern at these three wavelengths compared to the transform of the particle distribution does help to probe the phenomena. The direct comparisons reveal a number of details in the images that are not matched by a simplifying assumption of a single Gaussian transverse beam profile of the size consistent with the incoherent OTR measurements. Instead typically we need to use a split Gaussian with a smaller rms size to reproduce the fringe peak intensities in the vertical plane and the asymmetry in the horizontal and vertical angles for the 540-nm and 265-nm cases. These results indicate that there are localized transverse portions of the beam distribution with a higher bunching fraction than the mean. The different beam energies used in operating at three wavelengths result in different overlaps of the Fourier-transformed bunch form factor and the single-electron OTR angular distribution for a two-foil geometry. This aspect probes the model's applicability and sensitivities. We also provide evidence of the changes in the effective microbunching transverse radius from the exponential gain regime into the saturation regime. Finally, we recognize that the experimental COTRI patterns are not ideal, and that e-beam distributions and trajectory/coalignment issues are also part of the phenomena.

*Work supported by U.S. Department of Energy, Office of Basic Energy Sciences, under Contract No. W-31-109-ENG-38.
#lumpkin@aps.anl.gov

EXPERIMENTAL BACKGROUND

The experiments were performed at the APS SASE FEL facility. This facility includes the drive laser, S-band linac, bunch compressor, matching station, and the undulator hall with the UV-visible and VUV-visible diagnostics stations. Details have been reported previously [5] and most recently in these proceedings [6]. The emphasis in this paper will be on the description of the analytical model in the next section and comparisons to data in the subsequent section.

COHERENT OPTICAL TRANSITION RADIATION MODEL

Optical transition radiation (OTR) is generated when a charged-particle beam transits the interface of two media with different dielectric constants (e.g., vacuum to metal). The techniques have been more widely employed with electron beams, but so far only a few labs have looked at coherent OTR (COTR) and used COTR interferometry. Overall, the techniques provide information on transverse position, transverse profile, divergence and beam trajectory angle, emittance, intensity, energy, and bunch length. There are coherence factors for wavelengths longer than the bunch length and for microbunched beams such as those induced by a SASE FEL process.

It is this latter process that we have explored with the concomitant intense images. We use the model developed previously [4] to show the first direct comparisons of our COTRI data and calculations. The model describes the phenomenon in the spectral-angular distribution as a product of several functions as shown in Equation (1):

$$\frac{d^2N}{d\omega\, d\Omega} = \left| r_{\perp,\parallel} \right|^2 \frac{d^2N_1}{d\omega\, d\Omega} I\left(\boldsymbol{k}\right)\mathcal{F}\left(\boldsymbol{k}\right), \qquad (1)$$

where $r_{\perp,\parallel}$ are the reflection coefficients, $I(\boldsymbol{k})$ is the interference term, and $\mathcal{F}(\boldsymbol{k})$ is the coherence function. The single particle OTR distribution is

$$\frac{d^2N_1}{d\omega d\Omega} = \frac{e^2}{\hbar c}\frac{1}{\pi^2\omega}\frac{\left(\theta_x^2+\theta_y^2\right)}{\left(\gamma^{-2}+\theta_x^2+\theta_y^2\right)^2}, \qquad (2)$$

where the angles θ_x and θ_y are measured with respect to the angle of specular reflection, and $\frac{e^2}{\hbar c} = \alpha$ is the fine structure constant.

$I(\boldsymbol{k})$ is given by

$$I(\boldsymbol{k}) = 4\sin^2\left[\frac{kL}{4}\left(\gamma^{-2} + \theta_x^2 + \theta_y^2\right)\right], \qquad (3)$$

where L = the foil separation and $\boldsymbol{k}$ is the wave vector. The coherence function is given by

$$\mathscr{F}(\boldsymbol{k}) = N + N_B\left(N_B - 1\right)\left|H(\boldsymbol{k})\right|^2, \qquad (4)$$

where the bunching fraction $f_B = N_B/N$ and $H(\boldsymbol{k}) = \frac{\rho(\boldsymbol{k})}{Q} = g_x(k_x)g_y(k_y)F_z(k_z)$ is the Fourier transform of the charge form factors with Q = total charge of the micropulse. The transverse form factors are $g_i(k_i) = \frac{1}{\sqrt{2\pi}}e^{-\sigma_i^2 k_i^2/2}$, i = x,y, and the longitudinal form factor for a microbunch is $f(k_Z) = \frac{1}{\sqrt{2\pi}}e^{-\sigma_Z^2 k_Z^2/2}$.

The coherence function reduces to just the number of particles N when the number of microbunched particles N_B is zero. For the 540-nm case, we have f_B at 10 to 20% so the coherence enhancement of OTR is several orders of magnitude!

Besides tracking the z-dependent growth of COTR, the 540-nm COTRI patterns have an unusual sensitivity to electron beam size compared to OTR as shown in Fig. 1 for 220-MeV beam and 0.2 mrad divergence. Here, the different bunch form factors for 100-, 50-, and 25-µm size and 0.2% bunching fraction explicitly enhance different peak fringes. The smallest beam size with largest form factor in θ-space enhances the first three fringes compared to only the inner lobes for the 50- and 100-µm sizes. The sensitivity is less in the 100-, 150-, 200-µm regime as shown in Fig. 2, but there are still detectable differences. Basically the OTRI fringe peaks act as a built-in metric.

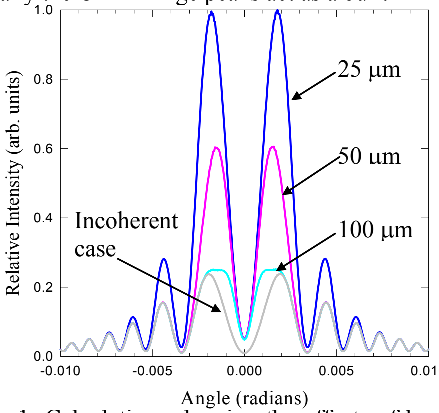

Figure 1: Calculations showing the effects of beam sizes of 100, 50, and 25 µm on the COTRI fringe peak relative intensities. A 220-MeV beam energy and 0.2 mrad divergence were used.

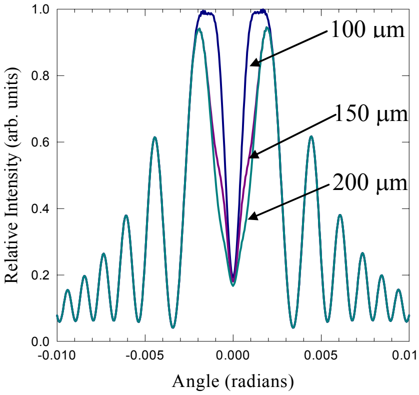

Figure 2: Calculations showing the effects of beam sizes 200, 150, and 100 µm on the COTRI fringe inner lobe relative intensities. The cofactors are narrow in angular space and only multiply the inner lobe distribution for this parameter set.

COMPARISONS OF DATA AND THE MODEL

540-nm Wavelength, Postsaturation Regime

The first case we wanted to study in more detail was the far-field image taken from the saturation regime in z after undulator 8 reported previously [2]. This particular image is very rich in features as we noted at that time. The most obvious effect after the reduced integrated intensity compared to data after undulator 5, is the difference in the θ_x and θ_y structure seen in Figs. 3 and 4, respectively. This is attributed to an elliptical e-beam and the corresponding asymmetric transform of the bunch form factor in θ-space. In the θ_y axis the presence of three fringe peaks versus the single inner lobe in θ_x is seen. The data in the exponential gain regime late in z do not exhibit three fringe peaks in any plane, so larger effective beam sizes are indicated.

The resulting calculations of the model using E = 220 MeV and $\sigma_{x',y'}$ = 0.2 mrad are directly compared in Fig. 3 for θ_x and Fig. 4 for θ_y. As the beam form factor is adjusted, it is clear that the shape of the first lobe is also sensitive to the effective beam size in the 50- to 100-µm σ_x size.

In the θ_x plane (Fig. 3), beam sizes of 75, 85, and 95 µm with a bunching fraction (BF) of 2% were evaluated. The first fringe peak at about ±1 mrad is narrower than that of the first θ_y peak. This is due to the larger effective σ_x, which transforms to a narrower bunch form factor in θ-space centered at θ = 0 so that only the inner side of the first lobe is involved in the products of Eq. (1).

When looked at closely, the vertical fringe pattern image has a slight tilt in the θ_x - θ_y plane so that our three-column-averaged profile does not hit the fringe peak at its maximum for both +θ_y and -θ_y values (Fig. 4). Attempts to match the asymmetry in peak intensities were made, but it appears that while σ_y = 20 µm works for fringe peaks 1, 3, and 4 at negative θ_y, the second fringe peak is overestimated. A σ_y = 25 μm value seems to give the correct height for peak #2, but it then misses the intensities for peaks 3 and 4.

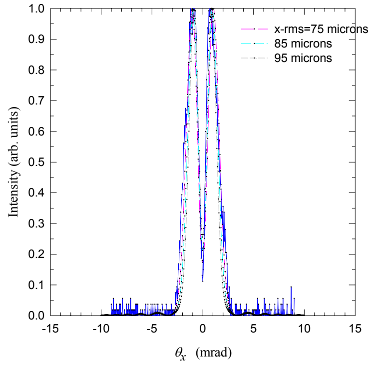

Figure 3: A direct comparison of model results with σ_x = 75, 85, and 95 μm and 2% bunching fraction and experimental θ_x data for the saturated regime case at 540 nm.

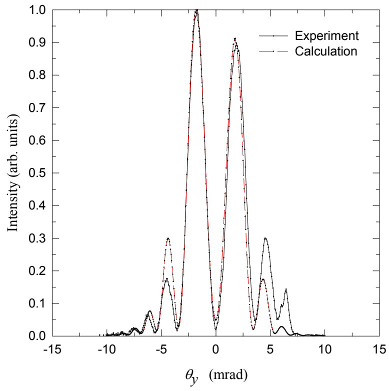

Figure 4: A direct comparison of model results and experimental θ_y data for the saturated regime case at 540 nm. A split Gaussian with 20-25 μm was used.

265-nm Case

The image to be examined was previously published as Fig. 3 of reference 7. The beam energy is now nominally 308 MeV.

The θ_x data are puzzling because although the two peaks fit in the envelope of the θ_y peaks, they do not match, as seen in Fig. 5. However, the peak locations match a calculation using the second harmonic wavelength at 132.5 nm as shown in Fig. 6. The $+\theta_x$ size is matched using σ_x = 20 μm, but the peak intensity symmetry is not matched. We suspect this is a beam coalignment or steering effect that is not in the model yet. We do not believe our 265-nm bandpass filters would pass the second harmonic, and furthermore, our camera is insensitive at 132 nm. There has been a report of second harmonic generation in a laser-field-accelerated electron beam [8], and there may be some related physics issues.

For this run, the effective beam size at this location seems to be elliptical with the major axis now on the y axis. This results in only seeing the two inner peaks with a valley depth between them consistent with $\sigma_{y'}$ = 0.1 mrad, BF = 2%, and σ_y = 35 μm as shown in Fig. 7.

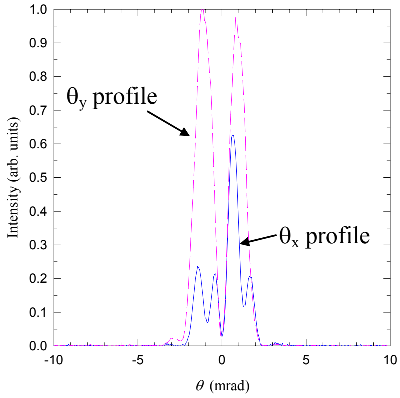

Figure 5: A comparison of the experimental θ_x and θ_y data for the 265-nm case.

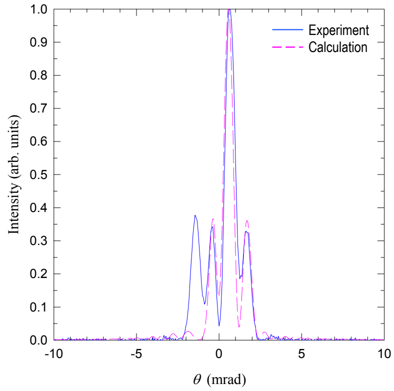

Figure 6: A direct comparison of model results and experimental θ_x data using the second harmonic wavelength of 132.5 nm.

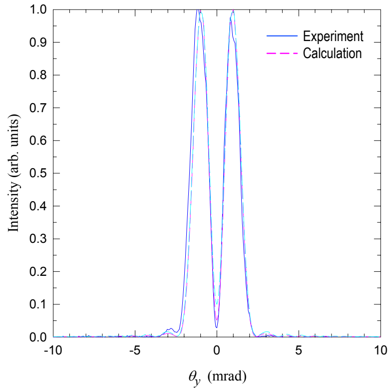

Figure 7: A direct comparison of model results at 265 nm for σ_y = 35 μm and two divergences (0.2 and 0.1 mrad). (The 0.1-mrad case has a deeper valley (red) like the data (blue)).

157-nm Case

The next wavelength regime used a new set of diagnostic stations to detect VUV radiation [5]. All optical transport is done with reflective optics. The beam energy is now 400 MeV, and the spherical mirrors are such that the camera only covers ± 2.5 mrad. At 400 MeV and L = 63 mm we calculate that the second fringe peak locations are at ± 2.0 mrad. This means that the majority of the detected information is in the first fringe peaks. We find that the bunch form factors and the narrower cone angle still result in sufficient sensitivity to beam size.

The image is somewhat like a four-leaf clover with four lobes of comparable intensity at 90° to each other. The fringe peak positions are different in θ_x and θ_y, and this we still attribute to the elliptical beam size. Only now the game is played on the first peak shape, not the visibility of the second or third fringe. The θ_x profile is matched with an asymmetric Gaussian of 43 μm and 25 μm for negative and positive angles, respectively, as shown in Fig. 8. The first peak location at 0.75 mrad is matched with the lobe width as well. There is a strong sensitivity of the lobe intensity to beam size in the $-\theta_x$ data where 43 μm matches better than 40 or 45 μm, but we probably also have an alignment effect as well.

The θ_y profiles and fringe peak positions at ± 0.5 mrad are matched with $\sigma_y \sim 50$ μm as seen in Fig. 9. The 40-μm calculation has too large of a lobe width and the 60-μm case mismatches the central minimum depth as well as the peak position.

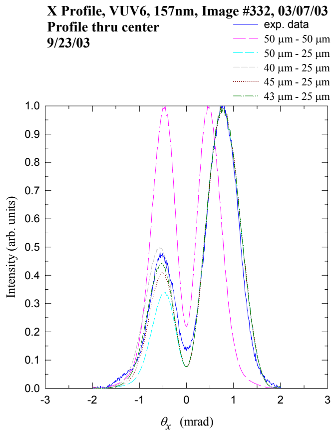

Figure 8: A direct comparison of the model results and experimental θ_x data at 157 nm. A split-Gaussian beam size is used to reproduce the asymmetry in the lobes and their peak positions.

SUMMARY

In summary, we have directly compared the results of a COTRI analytical model and data ranging from 540 nm to 157 nm corresponding to beam energies of 220 to 400 MeV. We have found that we can interpret fringe peak asymmetry in θ_x - θ_y in terms of beam size asymmetry in x and y. We also show that details involved in the ± θ_x or ± θ_y asymmetry can be reproduced with a split-Gaussian assumption for ± x or ± y beam profiles. COTRI has been shown to be a sensitive diagnostic of electron microbunch structure for the SASE process in the visible to VUV regimes. We expect that a similar formalism can be extended to the x-ray regime as discussed in another paper in these proceedings [9].

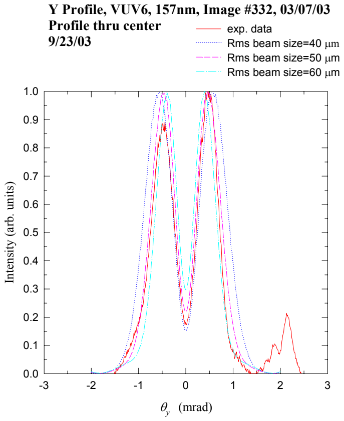

Figure 9: A direct comparison of model results for beam sizes of 40, 50, and 60 μm and the experimental θ_y data from VUV-6 at 157 nm. Best fit is for $\sigma_y = 50$ μm.

ACKNOWLEDGEMENTS

The authors acknowledge the support of Kwang-Je Kim and the Advanced Accelerator Research Initiative at Argonne National Laboratory.

REFERENCES

[1] A.H. Lumpkin et al., Phys. Rev. Lett. 86, 79 (2001).
[2] A.H. Lumpkin et al., Phys. Rev. Lett. 88, 234801 (2002).
[3] A.H. Lumpkin et al., "First Observations of COTR due to a Microbunched Beam in the VUV at 157 nm," Nucl. Instrum. Methods (in press 2004).
[4] D.W. Rule and A.H. Lumpkin, Proc. of the IEEE 2001 Particle Accelerator Conference, Chicago, IL, pp. 1288-1290 (2001).
[5] P. Den Hartog et al., Nucl. Instrum. Methods A483, 407 (2002).
[6] A.H. Lumpkin et al., "Use of VUV Imaging to Evaluate COTR and Beam-Steering Effects in a SASE FEL at 130 nm," these proceedings.
[7] A.H. Lumpkin et al., Nucl. Instrum. Methods A483, 402 (2002).
[8] S.D. Baton et al., Phys. Rev. Lett. 91(10), 105001-1 (2003).
[9] A.H. Lumpkin, William M. Fawley, and Donald W. Rule, "A Concept for z-dependent Microbunching Measurements with Coherent X-ray Transition Radiation in a SASE FEL," these proceedings.